Department of Physics and Astronomy
University of Heidelberg

Bachelor Thesis in Physics
submitted by

Felix Paul Gerhard Ziegler

born in Stuttgart (Germany)

2012

Kicked-rotor dynamics in optical fibers

This Bachelor Thesis has been carried out by Felix Paul Gerhard Ziegler at
the
Institute for Theoretical Physics in Heidelberg
under the supervision of
PD Dr. Sandro Wimberger

Abstract

In this thesis, we present theoretical investigations on a new view of the well-known quantum kicked rotor that has recently been realised in experiments at the Friedrich-Alexander University of Erlangen. In order to reproduce and explain experimental data, the wavefunction of a rotor confined in the angle space $[-\pi, \pi)$ is unfolded into position space by a modulation integral over the quasimomentum [1]. The central question of this thesis is motivated by experimental observations: How does the dynamics of the wave function that exhibits expansion or localisation depend on the kicking parameter? Based on numerical calculations, we present a theory on the dispersive behaviour of the dynamics depending on the kicking strength which is valid in a regime of small kicking parameters. Here, our main observable constitutes the expansion velocity of the wave function and we compare our results to Mathieu-theory and tunneling in periodic potentials.

Furthermore, we introduce the survival probability to stay in the Brioullin zone of the initial state which leads to a quantification how strong the wave function expands or localises dependent on values of a higher kicking parameter regime. It will be shown that we can reproduce experimental data by our numerical simulations and find observables to characterise the aforementioned expansion or localisation.

Zusammenfassung

In dieser Arbeit präsentieren wir theoretische Untersuchungen über eine neue Variante des bekannten quantenmechanischen gekickten Rotors, die kürzlich in Experimenten an der Friedrich-Alexander-Universität Erlangen realisiert wurde. Mit dem Ziel, die experimentellen Daten zu reproduzieren und zu erklären, wird die Wellenfunktion eines Rotors, die im Winkelraum $[-\pi, \pi)$ definiert ist, durch eine Phasenmodulation über den Quasiimpuls in den Ortsraum entfaltet [1].
Der zentrale Gegenstand der Untersuchungen dieser Arbeit is motiviert durch experimentelle Beobachtungen: Wie hängt die Dynamik der Wellenfunktion, die je nach Kickstärke Zerfaserung oder Lokalisierung aufweist, von diesem Parameter ab?
Basierend auf numerischen Rechnungen, präsentieren wir eine Theorie über das dispersive Verhalten der Dynamik in Abhängigkeit der Kickstärke, die in einem Regime für kleine Parameter gültig ist. Hierbei ist unsere grundlegende Observable durch die Ausbreitungsgeschwindigkeit der Wellenfunktion gegeben und wir ziehen zur Interpretation unserer Ergebnisse die Mathieu-Theorie über Tunneleffekte in periodischen Potentialen vergleichend heran.
Weiterhin führen wir die Überlebenswahrscheinlichkeit, in der Brioullinzone des Anfangszustands zu bleiben, ein. Dadurch ist es möglich, zu messen, wie stark die Wellenfunktion in Abhängigkeit der Kickstärke zerfasert oder lokalisiert. Hierbei untersuchen wir insbesondere einen Bereich für höhere Kickstärken. Es wird gezeigt, dass wir die experimentellen Daten durch unsere numerischen Simulationen reproduzieren und Observablen fnden, um die genannte Expansions- bzw. Lokalisierungsdynamik zu charakterisieren.

Contents

1 Introduction and Outline

Beginning with a theory to explain mechanics formulated by Hamilton and Newton, Henry Poincaré studied nonlinear perturbations of planetary orbits [2] and opened a door to a new field of physics in the 19th century: Nonlinear dynamics and classical chaos. This way of classical mechanics shows a huge range of applications in many fields such as statistical mechanics, hydrodynamics and astronomy, for example the Henon-Heiles problem in celestial mechanics [3], where for certain energies the considered system exhibits regular or chaotic motion, repectively.
At the beginning of the 20th century the development of quantum mechanics by Erwin Schrödinger, Werner Heisenberg and Paul Dirac, revolutionised physics. Consequently, the questions about chaos and nonlinear phenomenons occur also in quantum mechanics, which is originally formulated as a linear theory. The studies by Eugene Wigner in the past century have led to a definition of chaos in quantum systems which lies in the investigation of its spectral properties and considering that the classical corresponding system exhibits chaotic dynamics [4].
This thesis treats a famous and well-known nonlinear oscillator system which exhibits, dependent on certain parameter regimes, regular and chaotic dynamics and has both applications and realisations in classical and quantum mechanics: The kicked rotor. It consists of a simple rotator periodically driven by an external field. In classical mechanics the system is characterised by the standard map which is also called Chirikov-Taylor-map [5]. Its quantum version, the quantum kicked rotor (QKR), has been studied intensively in the past years [6]. It was found that the physics of the quantum kicked rotor is related to Anderson localisation in solid state physics [7]. Moreover, many experimental realisations of the QKR were established [8], such as the motion of cold atoms along a line. The kicking is caused by a standing laser wave which is switched on and off periodically in time. Newer experiments on kicked atoms can be found in [9].

Yet, there is a new interest motivated by recent experiments at the Friedrich-Alexander University of Erlangen. Those provide a realisation of the quantum kicked rotor by the propagation of a light signal in an optical fiber. The signal is modulated in time and periodically amplified which leads to a discrete kicking. Dependent on the kicking strength the signal exhibits two different

kinds of motion in time, which constitute the central focus of the experimentals. For some values of the kicking strength the signal localises in time and for others it disperses. Fig. 1.1 shows the propagation of several signals in time as a function of the kicking counter. Here, the initial states spread from their original zone to outer ones. Now the question is: Is it possible to describe this experiment by theoretical methods drawing back on known concepts of the kicked rotor? Are we able to understand the experimental structures and phenomena as a function of the kicking strength and is it possible to predict for a given kicking strength if there is expansion or localisation? To answer this question, we investiagte an observable that is known for some years but that has not been studied in detail yet. It is given by the wave function in position space $\psi(x)$ that results as a continuous superposition of Bloch waves (c.f. ch. 2), i.e. an integral over the quasi-momentum. The latter causes an unfolding and a modulation of the periodic wave function in angle space (rotor) to real space [1]. Since observations of the QKR dynamics typically take place in momentum space this observable is a non-standard way of investigating its dynamics. The crucial difference between experiment and theory lies in the fact that the experimental QKR localises or disperses in time, whereas in theory this takes place in real space. Furthermore, the modulation of the time evolved signal in the experiment stands in analogy to the unfolding of the wave function together with a modulation over the quasi-momentum. In the experiment a total of 40 values for the quasi-momentum have been reached so far.

In this thesis, we present a theory for the dynamics of the quantum kicked rotor in position space which is based on numerical calculations of the underlying kicked rotor model (c.f. ch. 4). In order to explain the experimental results, we focus on the dependence of the behaviour of the wave function on the kicking strength.Therefore, we introduce a numerical model to reproduce the experimental data and to analyse it. Here, we firstly consider small kicking parameters and investigate the expansion rate of $\psi(x)$, since in the experiment the spreading effect becomes smaller the higher the kicking strength is within this regime. To understand this phenomenon, we use the comparison with Mathieu-theory and tunnelling in periodic potentials. Secondly, we study the behaviour of the wave function in position space for higher values of the kicking parameter at which the phase space of the classical corresponding system exhibits mixed-regular and chaotic motion [2]. Here, we introduce the survival probability to stay in the zone of the initial state, because the dependence of the dynamics on the kicking parameter seems to be more arbitrary than for the small range. Finally, we introduce further tools to analyse the expansion and localisation dynamics in this mixed regular-chaotic regime.

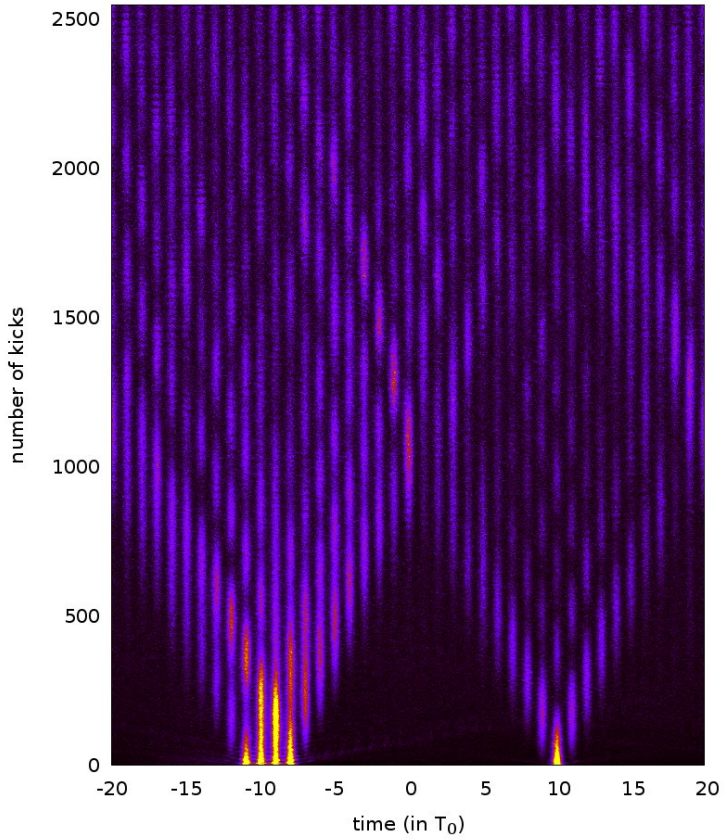

Figure 1.1: An experimental realisation of the quantum kicked rotor. The darker the color of the shapes in the contour plot the less intensity or probability density the single peaks show. This corresponds to a spreading of the initial wave packets in time. Since we want to understand the basic physics behind the experimental data, we consider only one initial state in our theoretical simulation similiar to that at $t = 10$. The picture was provided by courtesy of the experimental group of U. Peschel at the Friedrich-Alexander University of Erlangen.

2 Theoretical concepts

In this chapter, we introduce the fundamental theoretical concepts to describe the kicked rotor in classical and quantum mechanics. In section 2.1 the classical dynamics of the kicked rotor model are presented. Firstly, starting with the Hamilton function of the system we review the well-known standard map. Secondly, we investigate the properties of the underlying phase space for different system parameters. Section 2.2 contains a description of the corresponding quantum mechanical system. Here, we explain the quantum map introducing the time evolution operator of the system. Furthermore, two characteristic phenomena of the quantum kicked rotor are shown and compared to the classical system. In section 2.3 we present a description of the wave function of the quantum kicked rotor in position space which constitutes the central subject of focus in this thesis.

2.1 The Classical Kicked Rotor

2.1.1 The Standard Map

As mentioned in the introduction (c.f. ch. 1), a definition of quantum chaos lies in the comparison of a given quantum system with its corresponding classical system that shows chaotic behavior. Therefore, we present a short illustration of the classical kicked rotor which is discussed in detail in [2,10]. The Classical Kicked Rotor describes the motion of a particle confined to a circle which is periodically driven by an external field, as shown in fig. 2.1. In dimensionless units the Hamiltonian of the system is given by:

$$H(p,\theta;t) = \frac{p^2}{2} + k\cos(\theta)\sum_{j=-\infty}^{\infty}\delta(t-j\tau) \tag{2.1}$$

Here, k is the kicking strength and τ stands for the kicking period. Moreover $\delta(t-n\tau)$ is the Dirac delta distribution which represents the discrete kicking of the particle in regular time steps. Starting with Hamilton's equations of motion we are able to derive iterative equations in order to describe the time evolution of the (angular) momentum and the angular position of the particle.

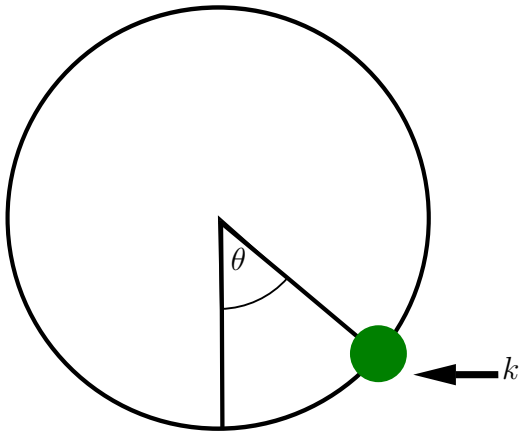

Figure 2.1: Model of a Classical Kicked Rotor: Motion of a particle with mass $m = 1$ on a circle kicked periodically by an external field

Hamilton's equations read:

$$\dot{p} = -\frac{\partial H(p,\theta;t)}{\partial \theta} = k\sin(\theta)\sum_{j=-\infty}^{\infty}\delta(t-j\tau) \tag{2.2}$$

$$\dot{\theta} = \frac{\partial H(p,\theta;t)}{\partial p} = p \tag{2.3}$$

In order to derive iterative equations for p and θ we need to integrate the equations of motion over one kicking period. Here, it is emphasised that the kick acts instantaneously. The angle of the particle stays constant during a kick whereas the momentum experiences a discontinuous change. During two kicks, i.e. over one kicking period, the angle changes continuously due to momentum conservation during the free time evolution. Integrating over one period we obtain the standard map [5, 11]:

$$p_{j+1} = p_j + K\sin(\theta_j) \tag{2.4}$$

$$\theta_{j+1} = \theta_j + p_{j+1} \mod (2\pi) \tag{2.5}$$

Here, the stochasticity parameter $K = k\tau$ was introduced. It is obtained by the substitution $(p \to \tau p)$ after integrating the equations of motion. In contrast to this, we will see in section 2.2 that the quantum kicked rotor is described by two control parameters, whereas in the classical case we only need K.

The stochasticity parameter K determines what kind of motion the particle on the circle shows, i.e. the structure of the phase space. Increasing K leads to a change from regular to chaotic phase space structures [2, 5].

2.1.2 Regular and chaotic motion

From equations (2.4) and (2.5) it follows that both p and θ show a periodicity of 2π. Therefore, we restrict the phase space into a cell with an area of $2\pi \times 2\pi$, thus the motion of the kicked particle in phase space is described by a toral map. For small stochasticity parameter (e.g. $K \approx 0.3$), which induces quasi regular dynamics of the system, the KAM-tori rest invariant under the external perturbation. If we increase the stochasticity parameter to $K = K_{\text{crit.}} \approx 0.972$, we observe that the torus, which corresponds to the separatrix of the classical pendulum (last KAM-torus), breaks and the remaining islands are surrounded by a chaotic sea. The islands around the first order fixed-point in $(0, 0)$ shrinks with increasing K and finally bifurcates. At this point, the island is stretched until it splits up into two islands around fixed-points of higher order [12]. For $K > 5$ a completely chaotic phase space remains, but tiny regular structures around the many fixed-points of higher orders can be found applying a high numerical resolution.

2.2 The Quantum Kicked Rotor

2.2.1 Floquet operator

The primary aim of this thesis is to investigate the quantum kicked rotor which has many important experimental realisations in atom optics such as laser-cooled atoms (sodium and cesium) driven by a standing laser wave [13, 14] which is switched on and off periodically in time in order to simulate the kicks. The standing wave induces a periodic potential which acts on the atoms. This experiment was firstly performed by Raizen and coworkers in 1999 [1, 8, 15]. In contrast to classical system described in section 2.1, the atoms which are kicked by the standing wave potential move on a line.

In SI-units the Hamiltonian of the quantum kicked rotor for a particle of mass m is given by:

$$\hat{H}' = \frac{\hat{P}^2}{2m} + V_0 \cos\left(\frac{2\pi}{a}\hat{X}\right) \sum_{j=-\infty}^{\infty} \delta(t - jT) \tag{2.6}$$

The amplitude of the standing wave is described by V_0 and a is the spatial period of the periodic potential. To rescale the given Hamiltonian in Bloch units we divide eq. (2.6) by $E_{\text{Bloch}} = 8E_r$, where $E_r = \frac{\hbar^2 k_r^2}{2m}$ stands for the recoil energy of a photon scattering off an atom [16]. This leads to the dimensionless Hamiltonian which reads:

$$\hat{H} = \frac{\hat{p}^2}{2} + k \cos(\hat{\theta}) \sum_{j=-\infty}^{\infty} \delta(t - j\tau) \tag{2.7}$$

Here we set $\theta = \frac{2\pi}{a}(x \mod (2\pi))$. Alternatively, we can write the Hamiltonian as follows:

$$\hat{H}'' = \frac{\hat{p}^2}{2}\tau + k\cos(\hat{\theta}) \sum_{j=-\infty}^{\infty} \delta\left(\frac{t}{\tau} - j\right), \tag{2.8}$$

where j represents the kick counter. In order to describe the time evolution of a quantum state the unitary Floquet operator is used which we construct via integration of the Hamiltonian in eq. (2.7) over the kicking period τ. Consequently, the Floquet operator determines the dynamics of a state from one kick to the following one. Thus, the time evolution is discretised by the kicks themselves and the state at time n is obtained by applying the Floquet operator n times to the initial state. The unitary Floquet operator consists of a part which corresponds to the kick and a free evolution term:

$$\hat{U} = \hat{K}\hat{F} = e^{-ik\cos(\hat{\theta})} e^{-i\tau\frac{\hat{p}^2}{2}} \tag{2.9}$$

In θ-representation the kicking operator $\hat{K} = e^{-ik\cos(\hat{\theta})}$ is in simple diagonal form whereas in momentum representation we find:

$$\langle p'| \hat{K} |p''\rangle = \int\int d\theta d\theta' \langle p'|\theta\rangle \langle\theta| e^{-ik\cos(\hat{\theta})} |\theta'\rangle \langle\theta'|p''\rangle = K_{p'-p''} \tag{2.10}$$

where $K_n = (-i)^n J_n(k)$ and the $J_n(k)$ are the Bessel functions of the first kind [17].

Now we introduce a model to link the particle moving along a line to the one on the circle known from the classical problem. At this, we use the spatial periodicity of the potential. The unitary operator $\hat{U}$ commutes with spatial translations by multiples of 2π. Due to the invariance of the potential with respect to spatial translation, this symmetry demands a conserved quantity. With the help of Bloch's theorem [18] we find that the latter is given by the quasi-momentum $\beta \in [0, 1)$ in the above dimensionless units and that we are able to write the wave function as a product of a 2π-periodic function and a plane wave. In general, this means that the wave function of a particle moving along a line can be described by a superposition of Bloch waves:

$$\psi(x) = \int_0^1 d\beta e^{i\beta x} u_\beta(x) \tag{2.11}$$

Here, $u_\beta(\theta) = u_\beta(\theta + 2\pi)$ holds, so the wave packet of the particle in position space is constructed as an unfolding of periodic functions which are defined on the circle, i.e. in the θ-zone $[-\pi, \pi)$. In other words we describe $\psi(x)$ as a continuous superposition of particles moving on the circle. From now, on we call those β-rotors with the wavefunction $u_\beta(\theta) = u_\beta(x \mod(2\pi))$.

The momentum can be written as $p := n + \beta$ where the quasi-momentum β is interpreted as the fractional part and n as the integer part of the momentum. Consequently, we need to redefine the Floquet operator for a β-rotor:

$$\hat{U}_\beta(t) = e^{-ik\cos(\hat{\theta})} e^{-i\frac{\tau}{2}(\hat{N}+\beta)^2} \tag{2.12}$$

Here, $\hat{N}$ represents the angular momentum operator (with eigenvalues $n \in \mathbb{N}$) which has the θ-representation $\hat{N} = -i\frac{d}{d\theta}$ with periodic boundary conditions [19].

2.3 The unfolded wave function in position space

In this thesis we want to simulate the wavefunction of the quantum δ-kicked rotor as obtained from Bloch's theorem in eq. (2.11). To achieve this, we start with a wave function of a single particle in the θ-zone, i.e. a β-rotor on the circle. As defined in section 2.2, $n \in \mathbb{N}$ describes the angular momentum eigenvalues corresponding to the basis of our Hilbertspace $\{|n\rangle\}$. As it can be found in various textbooks such as [18] a plane wave in θ-representation is given by:

$$\langle\theta|n\rangle = \frac{1}{\sqrt{2\pi}} e^{in\theta} \tag{2.13}$$

Furthermore we denote $|\psi\rangle$ the states of the particle that moves on a line in x-space and that we want to obtain as a superposition of β-rotors. The wave function of a β-rotor in θ-representation is defined as:

$$\langle\theta|\psi_\beta\rangle = \frac{1}{\sqrt{2\pi}} \sum_{n=-\infty}^{\infty} \langle n+\beta|\psi\rangle \, e^{in\theta} \tag{2.14}$$

This corresponds to a discrete Fourier-transformation from n-space to the θ-zone. Moreover the momentum representation of the β-rotor state is given by:

$$\begin{aligned}\langle n|\psi_\beta\rangle &= \int_0^{2\pi} \langle n|\theta\rangle \langle\theta|\psi_\beta\rangle \, d\theta = \frac{1}{2\pi} \int_0^{2\pi} \sum_{m=-\infty}^{\infty} e^{i(m-n)\theta} \langle m+\beta|\psi\rangle \, d\theta \\ &= \sum_{m=-\infty}^{\infty} \delta(m-n) \langle m+\beta|\psi\rangle = \langle n+\beta|\psi\rangle =: \langle p|\psi\rangle\end{aligned}$$

With help of the Fourier transformation and eq. (2.11) we obtain:

$$\int_0^1 d\beta e^{i\beta x} u_\beta(x) =: \psi(x) = \langle x|\psi\rangle = \frac{1}{\sqrt{2\pi}} \int_{-\infty}^{\infty} dp \, \langle p|\psi\rangle \, e^{ipx} \tag{2.15}$$

In our simulations we will compute the wave function $\psi(x)$ numerically following eq. (2.11) and (2.14). Our initial state is defined in the angular momentum

representation and is described by the same function for all β-rotors. The full time evolution for each β-rotor after t kicks is executed applying $\hat{U}_\beta$ from eq. (2.12) t times:

$$\psi_\beta(n,t) = \hat{U}_\beta^t \psi_\beta(n,0) \tag{2.16}$$

Then we apply the Fourier transformation eq. (2.14) to obtain $\langle\theta|\psi_\beta\rangle = u_\beta(\theta) = u_\beta(x)$ and finally obtain $\psi(x)$ using eq. (2.11).

In the follwing the initial unfolded wavefunction $\psi(x, t = 0)$ is calculated since it has a characteristic form and reappears in the time evolved wave function for certain values of the kicking strength as we will explain in chapter 4. Let $u_\beta(x,0) =: u(x)$ be the initial wavefunction which is identical for every value of β. Then it follows:

$$\psi(x) = \int_0^1 d\beta e^{i\beta x} u(x) = \frac{e^{ix}-1}{ix} u(x) \tag{2.17}$$

$$\Rightarrow |\psi(x)| = \left| \frac{\sin(\frac{x}{2})}{\frac{x}{2}} u(x) \right| = \left| \mathrm{sinc}\left(\frac{x}{2}\right) u(x) \right| \tag{2.18}$$

The here derived sinc-function plays an important role in classical wave optics, for example in the single slit experiment where it determines the intensity distribution of the diffraction pattern of coherent light.

In our numerical calculations we set the initial wave function $u_\beta(\theta)$ symmetrically around zero in the θ-zone $[-\pi, \pi)$. This is shown in fig. 3.1 in ch. 3 for a Gaussian wave packet, i.e. a coherent state with minimal uncertainty [18]. The time evolution and the unfolding of the wave function, in order to construct $\psi(x,t)$ according to eq. (2.11), imply that further zones on the x-axis, i.e. further wells in the periodic potential are occupied. This means that the probability density spreads depending on the kicking parameter k as we already mentioned in chapter 1. In other words, the spatial probability density changes in time and may flow from the central zone $[-\pi, \pi)$ to others. For a certain parameter regime in k we will use the survival probability to analyse the dynamics of the "kicked wave packet":

$$P_{\mathrm{surv}}(t) = \int_{-\pi}^{\pi} dx |\psi(x,t)|^2 \tag{2.19}$$

3 Methods

3.1 Numerical Methods

The foundation of our numerical simulations of the QKR model is formed by a Fortran95 programme. It contains the computation of the wave function in momentum space $\mathbb{R}$ and angle space $[-\pi, \pi)$. The latter is used to calculate the unfolded wave function described in eq. (2.11). Here, we focus on the numerical description of a single β rotor, whereas we describe the transition to $\psi(x)$ in the next section.

In all simulations the initial coherent state is set in momentum space which has a finite base of length $N = 2^m, m \in \mathbb{N}$. The fact that N has to be a power of two arises from the condition of the used Fast Fourier transformation [20,21] we need to switch between momentum and θ-space. To symmetrise the initial wave function in momentum space around the origin, we choose a discrete grid of $n = -\frac{N}{2}, -\frac{N}{2}+1, ..., \frac{N}{2}$. The initial coherent state has the shape of a Gaussian distribution which can be found in detail in [18]:

$$\psi(n, t=0) = \frac{1}{\sqrt{\sqrt{2\pi}\sigma_n}} \exp\left(-\frac{(n-n_0)^2}{4\sigma_n^2} - in\theta_0\right) \tag{3.1}$$

From eq. (3.1) it immediately follows that the Fourier transform $\hat{\psi}(\theta, t=0)$ has also a Gaussian shape and is centered around θ_0 in angle space. The latter is described by a grid $\theta_j = \frac{2\pi}{N} j$, where $j \in \{-\frac{N}{2}, ..., \frac{N}{2}\}$ In this thesis, we investigate the dynamics of the QKR whose Hamiltonian reads

$$\hat{H} = \frac{\hat{p}^2}{2} - k\cos(\hat{\theta}) \sum_{j=-\infty}^{\infty} \delta(t - j\tau) \tag{3.2}$$

which differs from eq. (2.7) only by a minus sign in the potential term. Consequently, the dynamics of the system is still the same if we shift the angle space $[0, 2\pi)$ by π to obtain the zone $[-\pi, \pi)$. Since we investigate the dynamics of an initial Gaussian state which is centered around the stable fixed point of the map deduced by eq. (2.1) , we choose $\theta_0 = 0$, so the initial state is set in the minimum of the negative cosine which can also be seen in fig. 3.1. Moreover we simulate the motion of a rotor, thus periodic boundary conditions for the wave function in angle representation are assumed for all times: $\psi(\theta = -\pi) = \psi(\theta = \pi)\ \forall t$.

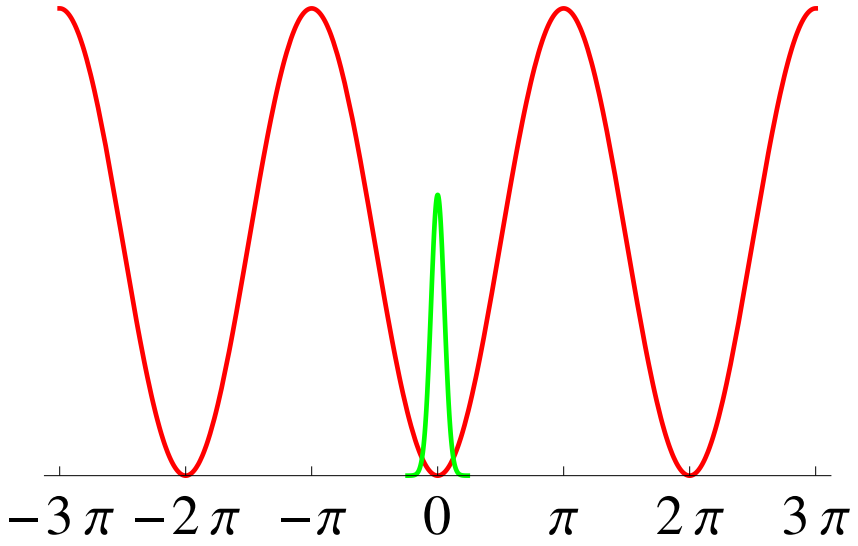

Figure 3.1: Initial state of a β-rotor set in the minimum of the negative cosine shaped potential.

Now, having a well-defined initial coherent state, we can start the time evolution of the rotor using the unitary Floquet-operator from eq. (2.12) $\hat{U} = \hat{K}\hat{F} = e^{ik\cos(\hat{\theta})}e^{-i\tau\frac{\hat{N}^2}{2}}$ as described in ch. 2. Here, we consider a rotor with $\beta = 0$ for the sake of simplicity. The time evolution of an initial state follows from eq. (2.16) and is given by:

$$\psi(t) = (\hat{U})^t\psi(0) \tag{3.3}$$

This can be performed numerically in a quite efficient way following these steps:

- Definition of the initial state $\psi(n, t = 0)$ in momentum representation
- Application of the free evolution operator $\hat{F}$ to obtain the state $\hat{F}\psi(n, t = 0)$
- Fast Fourier Transformation of the state $\hat{F}\psi(n, t = 0)$ into angle space $[-\pi, \pi)$
- Application of the kicking operator $\hat{K}$ to obtain the state $\hat{K}\mathcal{F}\left[\hat{F}\psi(n, t = 0)\right]$
- Inverse Fast Fourier Transformation back to momentum space to obtain the time evolved state $\psi(n, t = 1)$
- To obtain the time evolution up to any discrete time t, we have to repeat the described steps t-times.

The kicking operator $\hat{K}$ and the free time evolution realised by $\hat{F}$ are both in diagonal form in the θ- and n-basis respectively, thus the matrix multiplication on the defined vectors $\psi(j)$ and $\psi(\theta_j)$ reduce to scalar multiplications on each component with a phase $e^{-i\tau\frac{j^2}{2}}$ and $e^{ik\cos(\theta_j)}$, where $j \in \{-\frac{N}{2}, -\frac{N}{2}+1, ..., \frac{N}{2}\}$.

3.2 Simulation of the wavefunction in position space

Following the instructions from sec. 3.1 in order to compute the time evolved wave function of a rotor in momentum space, we now introduce the most important numerical concepts to obtain the unfolded wave function $\psi(x)$. Here we start with a set of N_β time evolved β-rotors with the wave functions $\psi_\beta(\theta, t) =: u_\beta(x \bmod(2\pi))$. Note that we are interested in the transition $\theta \to x$ for which the condition $\theta = x \bmod(2\pi)$ holds. Numerically we define the x-axis with the same resolution as the angle space and set $\Delta x = \Delta\theta = \frac{2\pi}{N}$. The aforementioned unfolding has to be computed for every point $x \in \mathbb{R}$ and we shortly explain the numerical solution to this.
Starting with the time evolved wavefunction $u_\beta(\theta)$ which is defined in $[-\pi, \pi)$, we expand the angle space to the whole real axis by writing the latter as a stringing together of many zones $[-m\pi, m\pi]$, where m is an even integer number. This is described by the following function:

$$g : [0, 2\pi] \to \mathbb{R}_{\text{num.}} : \quad \theta_j \mapsto \theta_j + 2\pi\left(l - \frac{N_{\text{zone}}}{2} - 1\right) \tag{3.4}$$

Here it holds, that $l = 1, ..., N_{\text{zone}}$, where $N_{\text{zone}} = 200$ was set in our simulations. From eq. 3.4 it follows that the real axis is simulated by an interval $[-\frac{N_{\text{zone}}}{2}\pi, \frac{N_{\text{zone}}}{2}\pi]$. Note again, that our initial state is centered around $0 \in [-\pi, \pi)$ and that there is a translation of π to the interval $[0, 2\pi)$ as it can be verified in fig. (6.1) in the appendix (c.f. ch. 6). The unfolding of the wave function is given by the integral from eq. (2.11) which reads:

$$\psi(x) = \int_0^1 d\beta e^{i\beta x} u_\beta(x), \tag{3.5}$$

where $u_\beta(x) = u_\beta(x + 2\pi)$ holds. Moreover, we write eq. 3.5 as a complex curve integral as it can be found in [22] and approximate it by a Riemann sum as shown in the following:

$$\int_0^1 d\beta e^{i\beta x} u_\beta(x) = \int_0^1 d\beta \cos(\beta x) u_\beta(x) + i\int_0^1 d\beta \sin(\beta x) u_\beta(x) \tag{3.6}$$

$$\approx \sum_{k=0}^{N_\beta - 1} \cos(\beta_k x) u_{\beta_k}(x)\Delta\beta_k + i\sum_{k=0}^{N_\beta - 1} \sin(\beta_k x) u_{\beta_k}(x)\Delta\beta_k, \tag{3.7}$$

where $\beta_k \in [0,1)$, $\Delta\beta_k = \beta_{k+1} - \beta_k = \frac{1}{N_\beta}$ and $k = 0, ..., N_\beta$. The expression in eq. (3.7) can be easily implemented in our Fortran95 code. In our investigations we chose $N_\beta = 100$ so that the deviation between the approximation above and the original integral over β is negligible. Furthermore, we note that the wave function $\psi(x)$ is normalised if the components $u_\beta(x)$ have a normalisation of one since we integrate over the unity interval $[0,1]$.

Moreover, we remark that the unfolding of the initial Gaussian wave function in angle space $[-\pi, \pi)$ which is centered around $\theta_0 = 0$ leads to a function of x that shows a periodicity of $N_\beta = 100$, which is a consequence of the modulation with phases $e^{i\beta x}$ for $\Delta\beta = \frac{1}{100}$. Fig. 3.2 visualises this showing an extract of the unfolded initial wave function of the coherent state over the numerical real axis consisting of 200 zones. Here, we observe that the wave function shows axial symmetry with respect to the origin and that the initial state lives with a probability of almost 1 in the central zone $[-\pi, \pi)$ corresponding to the angle space. Since we start with an equal initial state in θ-representation for each value of β, the squared absolute value of the wave function in position space is given by eq. (2.18) and has the form:

$$\psi(x, t=0) = \left| \frac{\sin(\frac{x}{2})}{\frac{x}{2}} \right|^2 \frac{1}{\sqrt{2\pi}\sigma_\theta} \exp\left(-\frac{(x \bmod(2\pi))^2}{2\sigma_\theta^2} \right) \tag{3.8}$$

3.3 Further techniques

The survival probability $P_{\text{surv}}(t)$ to stay in the central zone $[-\pi, \pi)$, described in eq. (2.19) is calculated by another Riemann sum over the unfolded wave function $\psi(x)$ at each discrete time t. Moreover, in order to obtain a qualitative comparison between experimental data as shown in fig. 1.1 and numerical simulations of the wave function, we used a Python script to create data of $\psi(x)$ at times between 0 and 2500 kicks. With the help of a Matlab programme a surface plot of the resulting graph containing the wave function in space and time can be made.

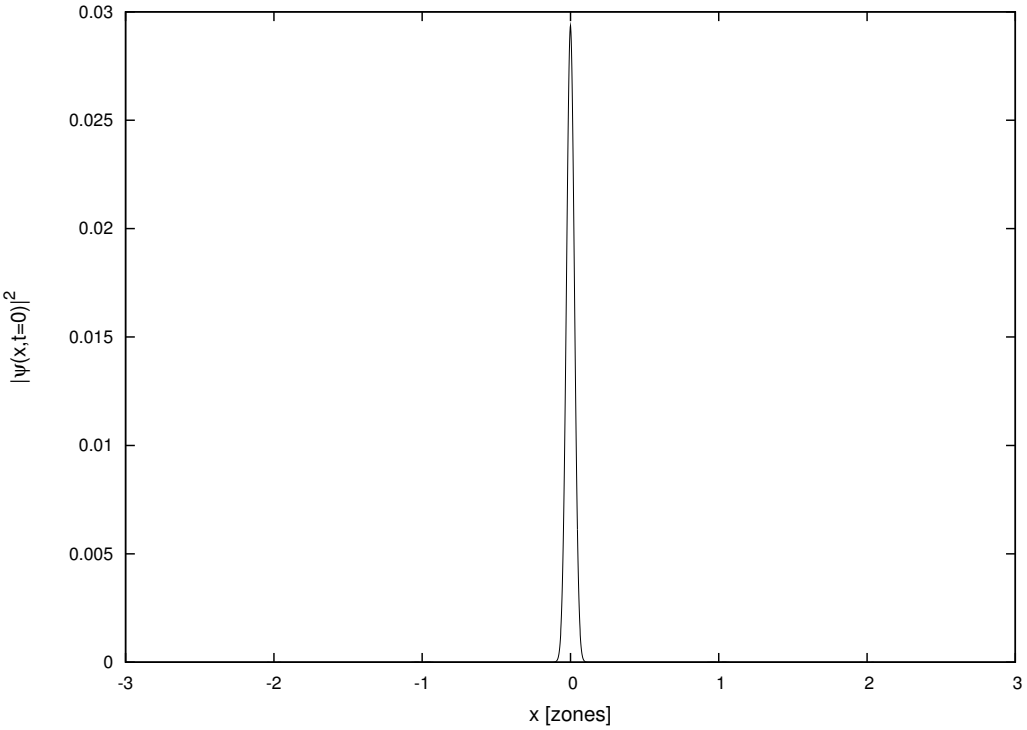

Figure 3.2: The unfolded initial wave function in position space. Due to its Gaussian shape it is symmetric around zero in accordance to its original representation in angle space. This picture shows only a small part of the wave function over 6 zones which have a width of 2π each.

4 Results

In this chapter we present our results on the investigation of the wave function in position space, which was motivated by experimental data from the Friedrich-Alexander University of Erlangen as described in ch. 1. All simulations were performed on the quantum kicked rotor model as described in ch. 2. In the experiments, the kicking period is held constant at the value $\tau = 0.66$, consequently the only control parameter is the kicking strength k. As it is easily seen from the experimental data, there are several ranges for the kicking strength k in which different kinds of dynamics take place.

Firstly, the dynamics for small k is investigated to compare experimental and theoretical results. Since for $k\tau < K_{\text{crit}}$ the corresponding classical phase space shows nearly-integrable, i.e. regular motion [12], we present a theory for the dispersion of the wave packet along the real axis using the approach of the classical pendulum. The results are compared to Mathieu-theory for tunnelling in periodic potentials. Secondly, we describe the dynamics for higher values of k where the classical phase space shows mixed regular-chaotic behaviour. Here, the survival probability to stay in the central zone as a function of k constitutes the main observable.

4.1 Dynamics for a small kicking parameter k

4.1.1 Comparison of experiment and theory

According to the description in ch. 3 we unfold the time evolved wave function from the θ-zone into position space following eq. (2.11) in order to study its dynamics dependent on the kicking strength k. Fig. 4.1 shows a comparison of experimental data and our simulations for $k = 0.24$ ($\tau = 0.66$). We directly observe that the theoretical model of the QKR is in good qualitative accordance with the results from the experiment. The color in the contour plots corresponds to the probability density of the wave packet. Both in the experimental data and in our simulation a characteristic pattern of the probability density up to 1000 kicks can be observed and the peaks with the highest intensity are located in the zones furthest away from the origin. For larger times the probability density in the theoretical simulation loses more and more intensity since the highest peaks have already drifted away from the considered

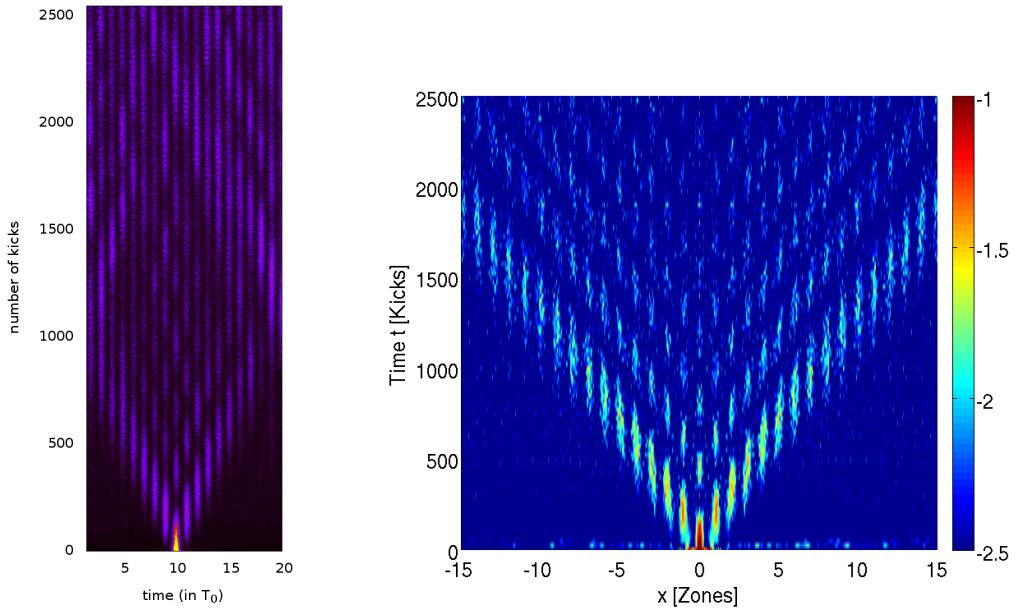

Figure 4.1: Spreading of the wave function for $k = 0.24$ ($\tau = 0.66$): a) The left picture shows experimental data describing the dynamics of an initial coherent state in the central zone. Here, we recall that time t in the experiment corresponds to position x in our notation as it was introduced in ch. 1. During the time evolution the state spreads and its maximal peak moves to outer zones. b) The picture on the right shows a simulation following the QKR model. Here we find a similar behaviour of the wave function in position space to the one that is observed in the experiment.

window of 30 zones on the real axis. In contrast to this monotonous behaviour the experimental data (left plot in fig. 4.1) show an increase of the probability density for large times and a breaking of the pattern which occurs until 1000 kicks. This phenomenon is due to interference of the state initially located at x=10 with the four, time evolved states which are initially located around x=0 as mentioned in ch. 1.

Fig. 4.2 shows simulations of the dispersion of the wave function in position space and we observe that the central peak survives longer the higher the kicking parameter k is set. The numbers of used quasi-momenta β for the unfolding integral and modulation are 40 in the experimental and 100 in the theoretical simulation (c.f. ch. 3). Moreover, β was chosen equidistantly from $[0, 1)$ and $\beta_0 = 0$ was set. To perform these simulation we recorded the data of the unfolded wave function for 100 time points between 1 and 2500 kicks. The contour plot was created to show the probability density dependent on time and position by using an interpolation function between the single snapshots. We conclude that for small parameters of k we can reproduce the experimental

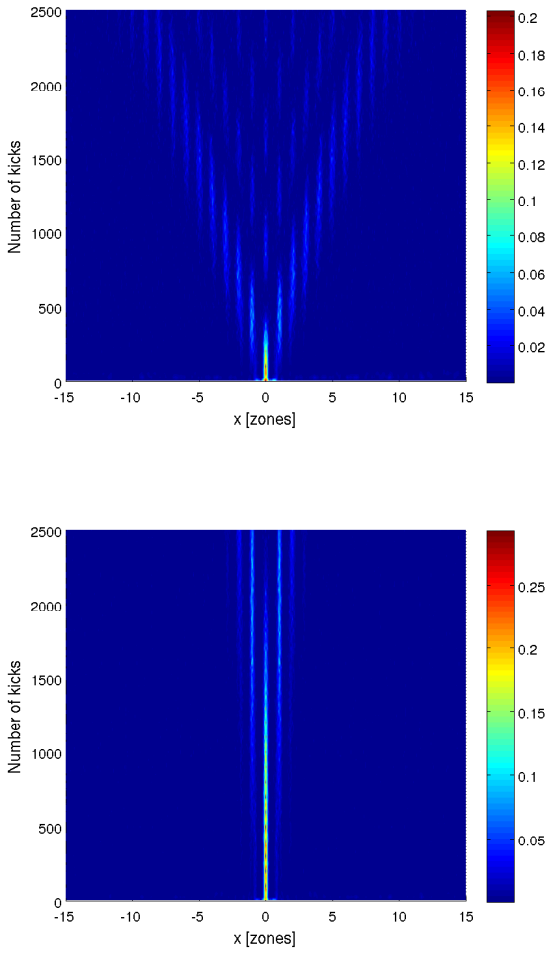

Figure 4.2: The spreading of the wave function in position space for a kicking strength $k = 0.36$ (upper plot) and $k = 0.66$ (lower plot), with $\tau = 0.66$ for each k.

data and observe that the spreading of the wave function decreases with higher values of k (c.f. fig. 4.2). For kicking parameters larger than $k \approx 0.5$ the wave function saturates in position space and the dispersion stops or moves very slowly until a time of 2500 kicks, respectively.

4.1.2 A quantitative theory for the dispersion dependent on k

The qualitative observations made in sec. 4.1.1 for $k \in [0.24, 0.5]$ lead to several questions. Firstly, why is the wave function spreading in position space and how does this phenomenon quantitatively depend on the kicking parameter k? Secondly, what exactly happens during this dispersion process, and why is

there a critical value of k at which the wave function essentially saturates in the central zone?

To answer the first questions we need to measure the spreading rate of the wave packet in dependence on the kicking strength k. In order to achieve this we determine the velocity of the highest peak of the unfolded wave function, i.e the part with the highest probability amplitude, as it can be well seen in fig. 4.3. This is numerically done by computing the unfolded wave function in

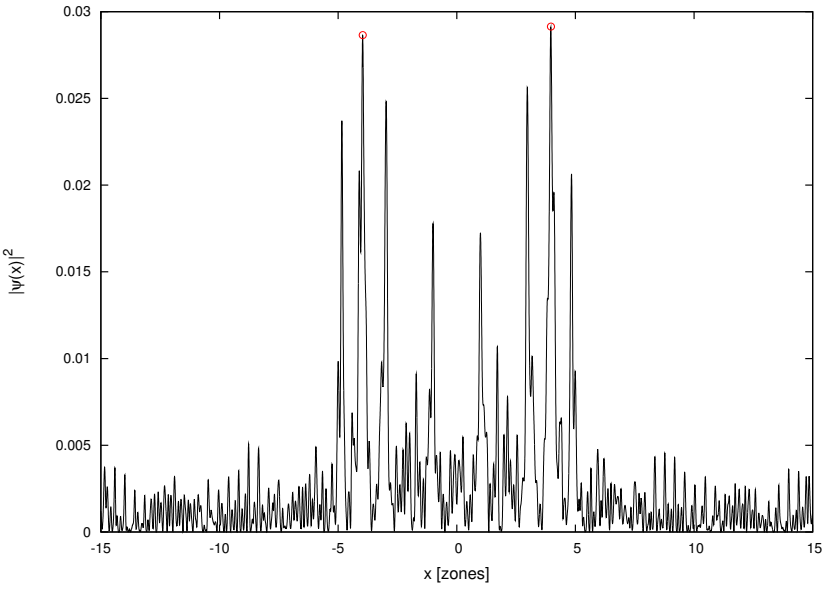

Figure 4.3: Unfolded wave function in position space after 550 Kicks for an initial Gaussian wave packet in the central zone. The position of largest the peaks (red circles) is determined in order to measure the spreading rate of the wave packet.

appropriate time steps in the window of 1 to 1500 Kicks and measuring the position of the maximum at each point in time. But this can be quite difficult because the peaks are oscillating with a period of about 10 kicks. Since the dispersion of the wave packet behaves quite linearly (which can be seen in fig. 4.1), we calculate the spreading rate , i. e. the dispersion velocity $v_{\text{disp}} = \frac{\Delta x}{\Delta t}$ from the slope of the resulting linear fit through the data points. The described process is repeated for different kicking parameters in the aforementioned range to obtain the spreading velocity as a function of k.
Now we know the quantitative behaviour of the dynamics of the wave function by having received several points of the velocity v_{disp} dependent on the kicking strength. But these results need to be explained by a physical model which we find by considering the corresponding classical phase space and the Hamiltonian of the kicked rotor system for the given range of k. At first, we

investigate the classical phase space showing regular motion for a stochasticity parameter $K = k\tau = k \cdot 0.66$ where $k \in [0.24, 0.66]$ as it can bee seen in fig. 4.4.

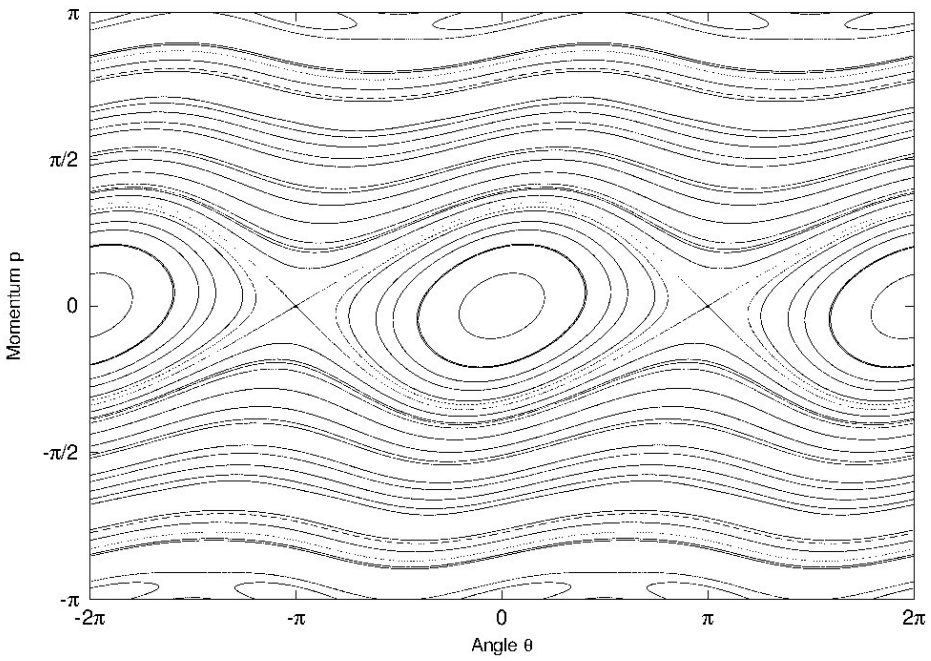

Figure 4.4: The phase space of the classical kicked rotor system for $K = k\tau = 0.3$ shows regular behaviour and the area within the separatrix possesses a similar structure to one of the classical pendulum.

The initial Gaussian wave packet in the θ-zone is centered around the stable fixed-point in (0,0) as shown in ch. 3. This corresponds to the minimum in the periodic kicking potential $V(\theta) = -k\cos(\theta)\sum_{j=-\infty}^{\infty}\delta(t-j)$, c.f. eq. (3.2). The motion of a particle along an orbit in phasespace as shown in fig. 4.4 corresponds to an oscillation process but in quantum mechanics a further possibility of motion lies in tunneling out of the classical barriers as it is described for example in [23, 24]. Consequently, a good candidate to explain the expansion of the wave function in time lies in the tunnelling of the wave packet out of the central zone (c.f. fig. 4.1).

In order to confirm this assumption, we need to find a comparable observable to our velocity v_{disp} as a function of the kicking parameter k. The required observable is given by the tunneling matrix element Γ which, as we will show, coincides with the spreading velocity v_{disp} with a certain accuracy. Since the Hamiltonian of the quantum kicked rotor contains a time-dependent potential it will be difficult to calculate the exact tunneling rate of the wave packet. But fortunately, for small kicking parameters $k \leq 0.5$ we can approximate the

classical phase space of the kicked rotor by the one of the pendulum as it can be clearly seen in fig. 4.4. Here, we emphasize that we consider an initial wave function located in the stable fixed-point, thus this approximation is valid in our problem. Moreover the Hamiltonian of the classical pendulum is given by [12]:

$$H(p,x) = \frac{p^2}{2} - V_0 \cos(x) \tag{4.1}$$

Here, V_0 denotes the strength of the external static field (e.g. gravity) and we note that there is no time dependence in eq. (4.1). Now, it is possible to obtain the tunneling rates from one potential well of the cosine to the next one. To achieve this, we need some help from Mathieu-theory for tunnelling in periodic potentials which we describe in detail in chapter 6. In order to compute the tunneling matrix element (or hopping coefficient) $\Gamma \equiv J_a$, we find the matrix representation of the given Hamiltonian:

$$\hat{H} = \frac{\hat{p}^2}{2} - V_0 \cos(\hat{x}),\ H(x+2\pi) = H(x) \tag{4.2}$$

Note that we investigate x which is a continous variable of the real axis. Using Bloch's theorem which is applicable on any Hamiltonian with a 2π-periodicity we obtain the following Schrödinger equation:

$$\hat{H}(x)\psi_\beta^\alpha(x) = E_\beta^\alpha \psi_\beta^\alpha(x), \tag{4.3}$$

where $\psi_\beta^\alpha(x)$ denotes a Bloch wave as defined in ch. 2 and α sets the index of the occupied energy band. We note that in our case α equals 1 since we investigate the tunneling of a particle in the ground state $|n\rangle$ from lattice site n to $n \pm 1$, where $n \in \mathbb{Z}$. Applying the tight-binding method on the Hamiltonian defined in eq. (4.2) we derive the tunneling matrix element $J_a = V_{nn'}$ as it follows [18]:

$$V_{nn'} = \langle n | H | n' \rangle = \int dx W_n^*(x) H(x) W_{n'}(x), \tag{4.4}$$

where we used the Wannier function $\langle x|n\rangle = W_n(x)$. Using the definition of the Wannier functions as the Fourier transforms of the Bloch waves we obtain the following result:

$$V_{nn'} = \langle \cos(k(n-n')) E_\beta^\alpha \rangle_\beta \in \mathbb{R} \tag{4.5}$$

$$V_0 = \langle E_\beta^\alpha \rangle_\beta \in \mathbb{R} \tag{4.6}$$

Thus the hopping coefficients are given by the average of the energy eigenvalues E_k^α modulated with a cosine and the tunneling matrix element J_a is determined by the width of the energy band in the Brioullin-zone.

Moreover, as it is reported in [25], for the tunnelling into the next nearest neighbour well it holds:

$$J_a \equiv \Gamma \propto e^{-c\sqrt{V_0}}, \tag{4.7}$$

where c is a constant perfactor. In the following we compare the measured velocity v_{disp} to the hopping coefficients. Firstly, it is important to match the quantity V_0 from eq. (4.2) with an appropriate one occuring in our model. At this, we consider the Hamiltonian of the QKR use the pendulum approximation which is valid for small values of k as τ is held constant:

$$H = \frac{p^2}{2} - k\cos(x)\sum_{j=-\infty}^{\infty}\delta(t-j\tau) \tag{4.8}$$

$$= \frac{p^2}{2} - \frac{k}{\tau}\cos(x)\sum_{j=-\infty}^{\infty}\delta(\frac{t}{\tau}-j) \tag{4.9}$$

$$\approx \frac{p^2}{2} - \frac{k}{\tau}\cos(x) \tag{4.10}$$

In the last step we used that the δ-function can be written as a series of plane waves which equals one in 0^{th} order. The hopping coefficients were numerically computed as a function of the parameter $\sqrt{\frac{k}{\tau}}$ where $\tau = 0.66$ and $k \in [0.24, 0.44]$, according to eq. (4.5) and (4.6). We compare them with the measured data points for the velocity v_{disp} with respect to eq. (4.7),

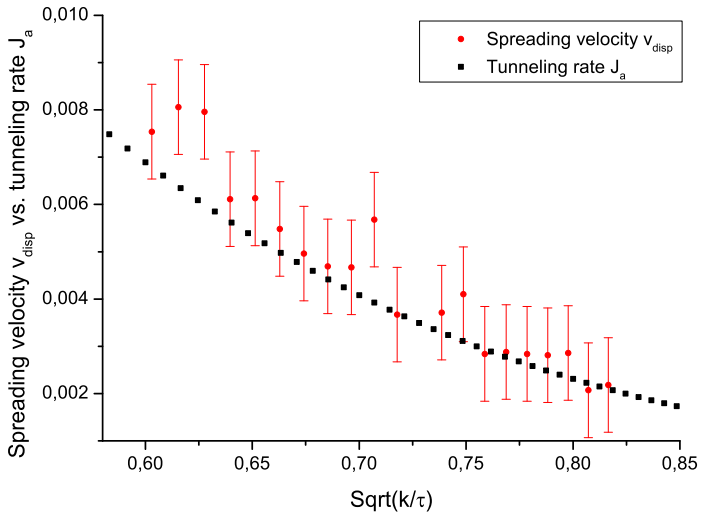

Figure 4.5: Comparison of the hopping coefficients J_a (black) which were numerically computed as a function of the parameter $V_0 = \sqrt{\frac{k}{\tau}}$ and the peak velocity v_{disp}.

From fig. 4.5 we observe an acceptable accordance between the simulation data and the values calculated from Mathieu-theory within the given error. The latter results from the graphic method of measurement as described above. An improvement of the measuring method would be to determine the "center of mass" of the highest peaks in the dispersing wave packet. But in order to explain the behaviour of the wave packet as a function of k, the values of v_{disp} provide a good approximation. Thus, we have found a quantitative model to explain the dispersion of the wave function in position space in a certain range of the kicking parameter k. The comparison with the tunnelling matrix elements J_a stays within its range of validity.

4.2 Dynamics in the mixed regular-chaotic regime

4.2.1 Comparison of experiment and theory

In the following, we investigate the dynamics of the wave function in position space for higher values of k keeping τ fixed as in our former considerations. Another interesting phenomenon, known from the experiment, occurs within the range $k \in [2, 4]$ where the wave function shows a systematic change of dispersion and localisation as a function of k. What makes this process worth being further investigated, is that a localisation can abruptly change to strong spreading dynamics et vice versa by a small change of the kicking strength ($\Delta k \lesssim 0.05$) as we see in fig. 4.6.
In contrast to section 4.1 , where we could find a continuous and regulary dependence of the dynamics on the kicking parameter, we do not find an obvious law of motion which the system obeys. We note that the wave function exhibits two different kinds of motion strongly sensitive to a small change in k. Despite, the simulation does not reproduce the experiment exactly. A systematic comparison between the experimental data and our simulations shows that there are slight shifts of the k values at which the spatial delocalisation and localisation change.
An explanation to this phenomenon could lie in the under- or overestimation of the kicking parameter k in the experimental setup as it has often occured in QKR experiments with cold atoms described in [26, 27].

4.2.2 A model of the dynamical behaviour of the wave function

In order to find a model to explain the remarkable dynamics of the wave function and its dependence on the kicking strength k, we need to describe

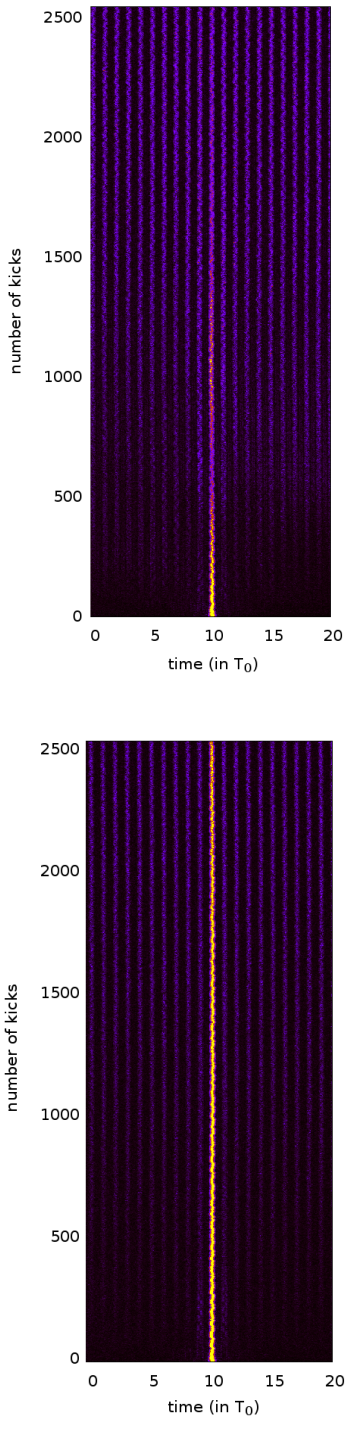

Figure 4.6: Experimental data for spreading (upper plot) and localisation (lower plot) of a wave packet in position space for higher values of the kicking parameter k. In the upper picture the kicking strength holds $k = 3.47$ and in the lower one $k = 3.55$. We observe a sharp change of the dynamics of the wave packet.

the occuring motion by an appropriate observable. As it turned out in the work underlying this thesis, the spreading velocity known from section 4.1 is useless because, in the aforementioned parameter regime of $k \in [2, 4]$, the wave function does not spread in the same way as it does for small kicking strengths. As we observed in our simulations, the central peak has a maximal probability amplitude if we neglect the oscillations which we mentioned in section 6.1. One may rather describe the dynamics of the wave packet as a form of probability loss to the other zones in the case of a value for k at which the wave function "defibrates". If localisation occurs probability is "conserved" in the central zone. Therefore an appropriate observable may be found in the probability to stay in the central zone $[-\pi, \pi)$ which is given by eq. (2.19).

$$P_{\text{surv}}(t) = \int_{-\pi}^{\pi} |\psi(x,t)|^2 dx \tag{4.11}$$

This observable was chosen because it replaces a spreading velocity and provides us with information how the wave function behaves at any point in time. Furthermore, it can be calculated quickly and ressource-efficiently by our numerics because we only need to integrate the probability density over the central zone. Other equivalent methods would be the measurement of the probability of presence in the whole position space without the central zone where the integral above is executed over $\mathbb{R} \setminus [-\pi, \pi)$. But obviously this yields exactly $1 - P_{\text{surv}}(t)$. Another observable is given by measuring the overlap of the time evolved wave function $|\psi(t)\rangle$ in the central zone with the initial state $|\psi(t = 0)\rangle$, which differs from the first mentioned method by the fact that it measures a relative probability or fidelity (c.f. [28]) compared to the initial state.

As it follows in fig. 4.7, we show our results for the observable $P_{\text{surv}}(t)$ which we computed over a time of 2500 kicks and a range of 92 parameters for the kicking strength $k \in [2, 4]$ where we set $\tau = 0.66$. In order to identify the most important aspects of the dynamics, only several graphs of $P_{\text{surv}}(t)$ are shown which reflect a characteristic dependence on the kicking strength. For some values of k the probability function $P_{\text{surv}}(t)$ shows strong oscillations as it can be seen in the picture in the upper left corner in fig. 4.7. This is assumed to be the same phenomenon that was described in sec. 6.1, caused by oscillations of the probability density within the central zone. Moreover, we can identify a dramatic change of the survival probability for certain values of k. For example the central picture in the upper row and the one in the lower left corner show localisation of the wave function in the central zone, whereas the pictures in the upper right and the central one in the lower row exhibit minima in the survival probability. The latter corresponds to a spreading of probability to the outer zones. For kicking strengths in the range $3.77 \leq k \leq 3.95$, an almost

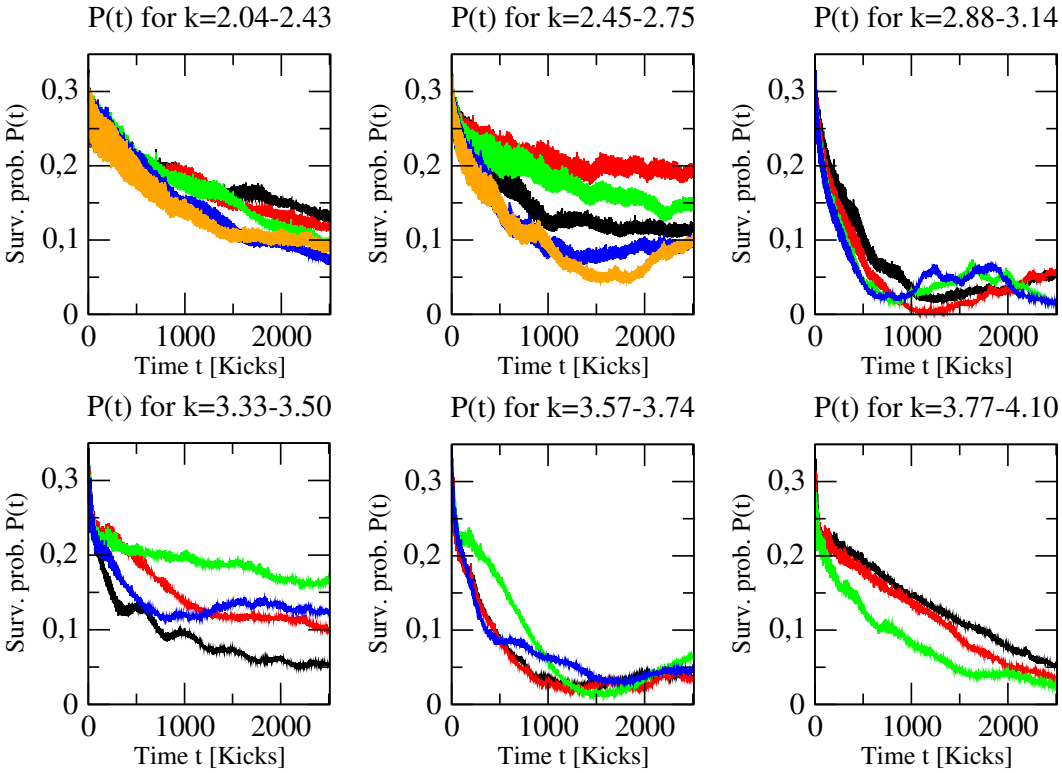

Figure 4.7: The survival probability $P_{\text{surv}}(t)$ was computed for many values of the kicking parameter $k \in [2, 4]$ and one can observe sharply different kinds of motion for certain parameter ranges. For example the red curve in the central picture of the upper line shows localisation of the wave function in the central zone, whereas in the picture in the upper right corner a minimum around a time of 1200 kicks occurs which corresponds to a dispersion of the wave function. The order of the plots following an increasing k is given by: black, red, green, blue, orange.

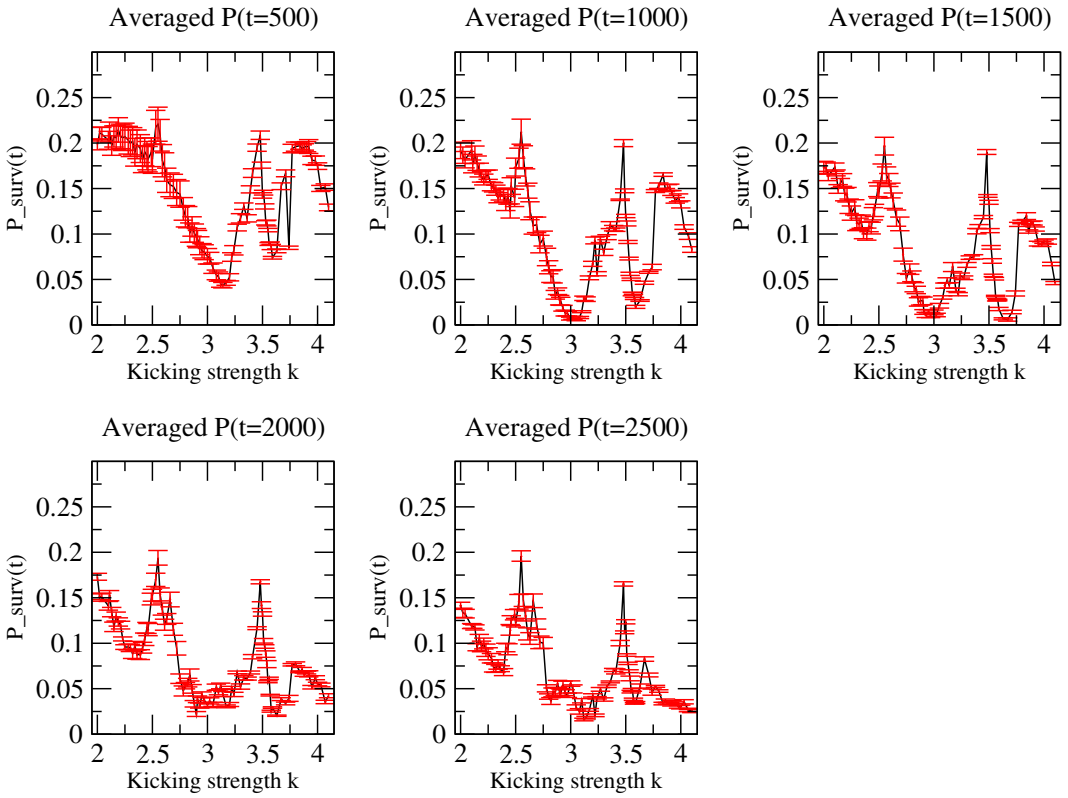

Figure 4.8: These diagrams show the survival probability to stay in the central zone for different times at $\tau = 0.66$ and as a function of the kicking strength k. There are two main peaks where the wave function localises at $k \approx 2.5$ and $k \approx 3.5$. These peaks are clearly dominant for times larger than 1500 kicks. On the other hand a spreading of the probability density occurs for $k \gtrsim 3$ where a minimum is observable that is minimal for about 1000 kicks. The shown range $k = 2, ..., 4$ corresponds to a stochastic parameter $K = k\tau \approx 1.33, ..., 2.66$.

linear decrease of the survival probability occurs. The figures shown here, illustrate a good accordance with the experimental results.

To obtain a deeper understanding of this observable, we will consider the average survival probability as a function of the kicking parameter k at certain time steps averaged over a small time interval, $\Delta t \approx 10$ kicks, for the reason of the mentioned oscillations. Following this we obtain the diagrams shown in fig. 4.8 which were created for cuts at the times 500, 1000, 1500, 2000 and 2500 kicks using the data which was plotted in fig. 4.7. From fig. 4.8 we obtain characteristic maxima of $P_{\text{surv}}(t)$ at $k \approx 2.5$ and $k \approx 3.5$ which correspond to localisation whereas the minimum around $k \approx 3$ means a spreading of the probability density out of the central zone. But the most important result is

the following: The kind of motion the system exhibits in the considered parameter range $k \in [2, 4]$ is not only dependent on the kicking strength but also on time itself.

Finally, we consider the classical phase space for the parameter range of $k \in [2, 4]$. Since $\tau = 0.66$, the critical value K_{crit} is already exceeded and the phase space of the classical kicked rotor exhibits mixed-regular and chaotic behaviour. The phase space corresponding to the value $K = k\tau = 2.04 \cdot 0.66 = 1.3464$ was computed and is presented in fig. 4.9. As mentioned in chapter 2, the classical

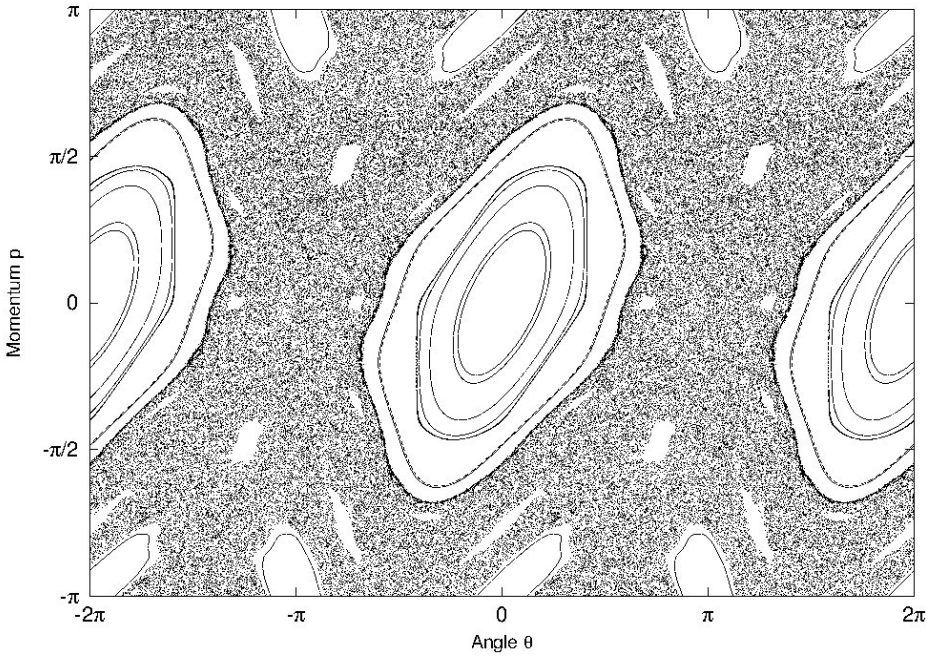

Figure 4.9: The classical phase space shows mixed-regular and chaotic behaviour for $K \approx 1.346$.

phase space has the only control parameter $k\tau$. Therefore, a possible way to find out if the behaviour of the wave function in position space is caused by classical or quantum mechanical effects lies in the variation of k and τ keeping the stochasticty parameter K constant. We computed numerically a further data set of $P_{\text{surv}}(t)$ (and the corresponding cuts at fixed times, as shown in fig. 4.10) for the range of $k \in [1, 4]$ and fixed kicking period $\tau = 1$ as it is set in the experiment. Unfortunately, there are no experimental data yet with which we can compare our results from the simulations presented in fig. 4.10. But we remark that the dependence of the survival probability on k for $\tau = 1$ differs from the one we obtained for $\tau = 0.66$ considering the range where $k\tau = \text{const}$. From fig. 4.10 it follows that the survival probability shows two characteristic peaks (around $k \approx 2.5$ and $k \approx 3.5$) which slightly shrink in time, whereas its behaviour for larger kicking strengths indicates (apart from a localisation

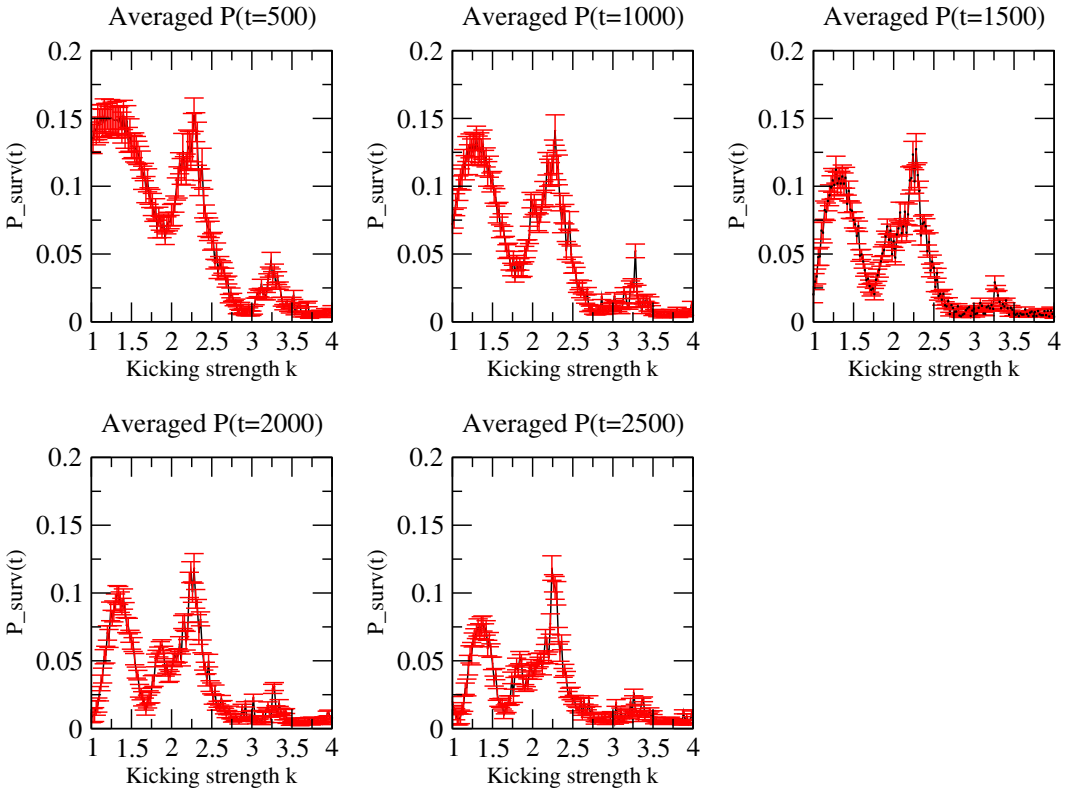

Figure 4.10: The survival probability at different times for $\tau = 1$ as a function of the kicking strength k. Here, the range of k corresponds to $K = k\tau \approx 1, ..., 4$.

peak at $k \approx 3.25$) a dispersion of the wave function in position space. Here, we note that for $K = 4$ the corresponding classical phase space is already strongly chaotic (up to regular structures remaining from the central island).

Since the classical dynamics is only governed by the stochastic parameter $K = k\tau$, we plot the data from fig. 4.8 and fig. 4.10 together as a function of K for 500 and 2000 kicks (c.f. fig. 4.11). Using this, we may better analyse the overlapping regions for the different kicking periods.

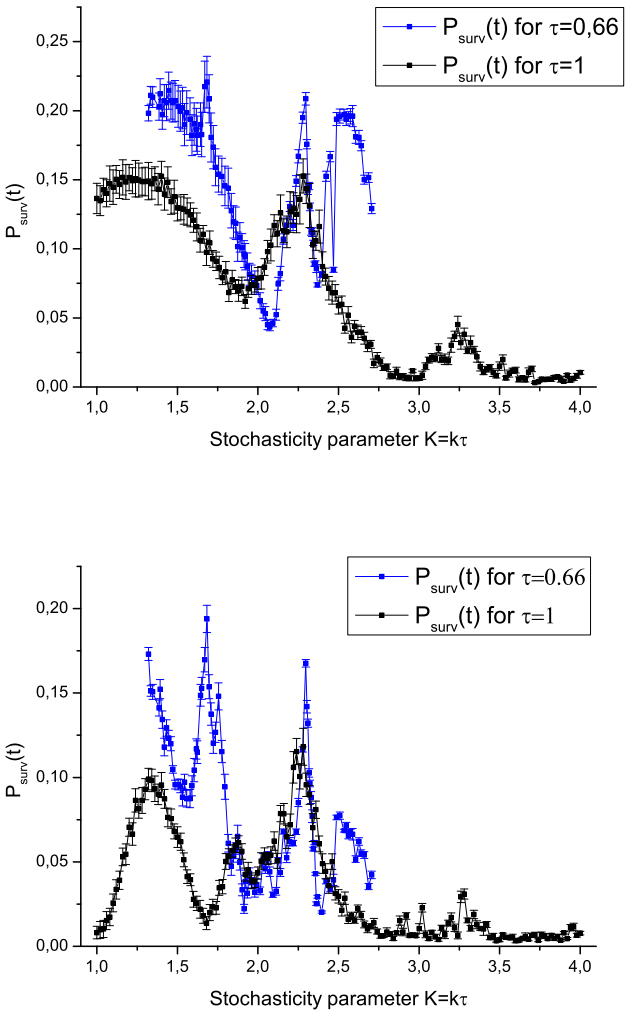

Figure 4.11: The two diagrams show the rescaled survival probabilities from fig. 4.8 and fig. 4.10 as a function of the stochastic parameter $K = k\tau$. The blue curve corresponds to the probability for $\tau = 0.66$ and the black curve to $\tau = 1$. The upper diagram belongs to cuts at 500 and the lower one to those at 2000 kicks.

Moreover, we present the positions of the maxima on the k- and $k\tau$-axis respectively in tab. 4.1. We notice that for the position $k\tau \approx 2.3$ the maxima in

τ	k			$K = k\tau$		
0.66	2.5	3.5	3.75	1.7	2.3	2.5
1	1.25	2.25	3.25	1.25	2.25	3.25

Table 4.1: Positions of the maxima in the diagrams in fig. 4.8 and fig. 4.10 dependent on the kicking parameter k and the stochasticity parameter $K = k\tau$.

fig. 4.8 and fig. 4.10 almost coincide and consequently the classical phase space seems to be responsible for this. On the other hand, we cannot find a good accordance between the other peaks. Finally, we note that for $\tau = 1$ the survival probability is smaller than for $\tau = 0.66$ in general, thus tunneling effects become stronger with increasing τ, which is our effective $\hbar$, i.e. it determines how many quantised states are set in a given phase space volume.

5 Conclusion and Outlook

In this thesis we investigated a variant of the quantum kicked rotor model which has been realised in recent experiments. In order to explain experimental results on the dynamics of the wave function in position space and especially its dependence on the kicking parameter k we performed the unusual unfolding of the wave function as a continuous superposition of Bloch waves following eq. (2.11).
In the first part of our evaluation of the numerical data we introduced the dispersion velocity v_{disp} as a significant observable in order to measure the quantitative dependence of the spreading of the wave function for small values of the kicking parameter. Here, the essential assumption lies in the approximation of the standard map by the well-known classical phase space of the pendulum, which is valid for small $k\tau$. Using this ansatz we were able to compare the spreading velocity v_{disp} with the hopping coefficients J_a which are obtained from Mathieu-theory as it is shown in chapter 6. This confirms that the spreading at small k is caused by a tunneling process in the periodic phase space along the $x-$direction.

In the second part we considered a regime of larger kicking parameters for the fixed kicking period $\tau = 0.66$. Also here, we observe good qualitative accordance of our numerical simulations with the experimental data. In order to describe the dynamics and its behavior with respect to small changes in the kicking strength, the survival probability $P_{\text{surv}}(t)$ was defined to measure the amount of probability which stays in the central zone and which flows to the outer ones during the temporal evolution for certain values of k.
Since a straightforward functional dependence of the dynamics on k was not found, more quantities have had to be involved in our computations. We compared our data corresponding to $\tau = 0.66$ with further numerical simulations of the same kind with a varied effective Planck constant τ. From the so far analysed data we can assume that the behaviour of the wave function in position space in the given parameter regime is influenced by the classical phase space (c.f. tab. 4.1). Moreover, we expect that the more τ is decreased the more classical the dynamics becomes and tunneling will be suppressed. In general, more data for different values of τ should be produced and analysed, since no mechanics - neither classical nor semiclassical, for the structure of the main observable $P_{\text{surv}}(t)$ could be found.

A possible mechanism may be resonant-assisted tunneling which is mediated by classical resonances of higher-order within the main pendulum like island in phase space (around the stable fixed-point) [24]. Further influences may lie in coherent destruction of tunneling as it can be found in [29].

6 Appendix

6.1 Derivation of the hopping coefficients J_a

The Hamiltonian of the system is given by:

$$\hat{H} = \frac{\hat{p}^2}{2} - V_0 \cos(\hat{x}) = \frac{1}{2}\frac{\partial^2}{\partial x^2} - V_0 \cos(\hat{x}), \quad H(x + 2\pi) = H(x) \tag{6.1}$$

The energy eigenvalue equation is given by:

$$\hat{H}(x)\psi_k^\alpha(x) = E_k^\alpha \psi_k^\alpha(x), \tag{6.2}$$

where the functions $\psi_k^\alpha(x)$ are Bloch waves which can also be written as $\psi_k^\alpha(x) = e^{ikx}u_k^\alpha(x)$. Here, α denotes the band index. In order to derive the tunnelling matrix element, i.e. the hopping coefficient J_a which determines the tunnelling rate of a particle from site n to site $n \pm 1$ in the periodic potential. Let the ket $|n\rangle$ be the groundstate of the particle localised at the lattice site n, i.e. the Wannier state. Using this we can write the Hamiltonian in matrix form:

$$\hat{H} = \sum_{n,n'} |n\rangle \langle n| \hat{H} |n'\rangle \langle n'| = \sum_n E_n |n\rangle \langle n| + \sum_{\langle n,n'\rangle} V_{nn'} |n\rangle \langle n'| + h.c. \tag{6.3}$$

The $\langle n, n'\rangle$ index means that the sum runs over the nearest neighbours. This is the well-known tight-binding approximation which is described in detail in Sakurai (c.f. [18]) or other textbooks. The interesting part of the Hamiltonian is $\sum_{\langle n,n'\rangle} V_{nn'} |n\rangle \langle n'|$ since it stands for the leakage of particles to the neighbouring lattice sites due to tunnelling. Therefore $V_{nn'}$ determines the tunnelling matrix element J_a and can be computed as follows:

$$V_{nn'} = \langle n| \hat{H} |n'\rangle = \int dx \int dx' \langle n|x\rangle \langle x| \hat{H} |x'\rangle \langle x'|n'\rangle \tag{6.4}$$

$$= \int dx \langle n|x\rangle H(x) \langle x|n'\rangle \tag{6.5}$$

$$= \int dx W_n^*(x) H(x) W_{n'}(x), \tag{6.6}$$

where the identity $\int dx |x\rangle \langle x| = \mathbf{1}$ was used. In the last equation we used the Wannier function $\langle x|n\rangle = W_n(x)$. They are defined as the Fourier transforms of the Bloch waves:

$$W_n(x) = \int_{-\frac{1}{2}}^{\frac{1}{2}} dk e^{-ikn} \psi_k^\alpha(x) \tag{6.7}$$

It follows for the coefficients $V_{nn'}$:

$$V_{nn'} = \int dx \int_{-\frac{1}{2}}^{\frac{1}{2}} dk \int_{-\frac{1}{2}}^{\frac{1}{2}} dk' e^{ikn} e^{-ik'n'} \psi_k^{*\alpha}(x) \hat{H} \psi_{k'}^{\alpha}(x) \tag{6.8}$$

$$= \int dx \int_{-\frac{1}{2}}^{\frac{1}{2}} dk \int_{-\frac{1}{2}}^{\frac{1}{2}} dk' e^{ikn} e^{-ik'n'} \psi_k^{*\alpha}(x) E_{k'}^{\alpha} \psi_{k'}^{\alpha}(x) \tag{6.9}$$

$$= \int_{-\frac{1}{2}}^{\frac{1}{2}} dk \int_{-\frac{1}{2}}^{\frac{1}{2}} dk' e^{ikn} e^{-ik'n'} \delta(k-k') E_{k'}^{\alpha} \tag{6.10}$$

$$= \int_{-\frac{1}{2}}^{\frac{1}{2}} dk e^{-ik(n'-n)} E_k^{\alpha} \tag{6.11}$$

$$= \int_{0}^{\frac{1}{2}} dk e^{-ik(n'-n)} E_k^{\alpha} - \int_{0}^{-\frac{1}{2}} dk e^{-ik(n'-n)} E_k^{\alpha} \tag{6.12}$$

$$\underbrace{=}_{k \to -k} 2 \int_{0}^{\frac{1}{2}} \cos(k(n-n')) E_k^{\alpha} dk \tag{6.13}$$

Consequently, the hopping coefficients are given by the following mean values [30]:

$$J_{nn'} = \langle \cos(k(n-n')) E_k^{\alpha} \rangle_k \in \mathbb{R} \text{ due to the relation } E_k^{\alpha} = E_{-k}^{\alpha} \tag{6.14}$$

$$J_0 = \langle E_k^{\alpha} \rangle_k \in \mathbb{R} \tag{6.15}$$

Note on the matrix representation of $\hat{H}$:
The matrix representation of $\hat{H}$ in eq. (6.3) can be derived using the $\{|n\rangle\}$ basis. We consider the potential part of the Hamiltonian.

$$V_{nn'} = \langle n|\hat{V}(x)|n'\rangle = -V_0 \int dx \int dx' \langle n|x\rangle \langle x|\cos(\hat{x})|x'\rangle \langle x'|n'\rangle \tag{6.16}$$

$$= -V_0 \int dx e^{ix(n-n')} \cos(x) \tag{6.17}$$

$$= -\frac{V_0}{2} \int dx \left[e^{ix(n-n'+1)} + e^{ix(n-n'-1)} \right] \tag{6.18}$$

$$\propto [\delta_{n,n'-1} + \delta_{n,n'+1}] \tag{6.19}$$

From the last equation (6.19) the tridiagonal structure of eq. (6.3) is obtained, where the kinetic term of eq. (6.1) determines the diagonal elements.

6.2 Fast Fourier transformation

As it was described in ch. 3 the numerical computation of the quantum kicked rotor requires the use of a discrete Fourier transformation which is applied on the vector components of the defined wave function $\psi(n)$ in momentum and

$\psi(\theta_n)$ in angle space respectively (n=1,...,N). [21] provides a very clear illustration of the discrete Fourier transformation and we present a short summary in the follwing.

Given a discrete periodic function $f : \mathbb{R} \to \mathbb{C}, t \mapsto f(t)$ over an equidistant grid $t_k = k\Delta t$, where $k \in \mathbb{Z}$ and $\Delta t \in \mathbb{R}_+$ with a period T for which it holds $T = N\Delta t$, $N \in \mathbb{N}$. Now we can write the N values of f in a unique vector representation $y \in \mathbb{C}^N$ with components $y_j = f(j\Delta t)$ and set $T = 2\pi$ without loss of generality since T does not appear in the Fourier coefficients of f. For the Fourier coefficients of y it holds:

$$c_k := \frac{1}{2\pi} \sum_{j=0}^{N-1} y_j e^{-i\frac{2\pi}{N}kj} \Delta t, \quad k = 0, 1, ..., N-1 \tag{6.20}$$

This definition induces a bijective linear function DFT : $\mathbb{C}^N \to \mathbb{C}^N$, which is called discrete (finite) Fourier transformation (DFT) and has an inverse function which is called inverse discrete Fourier transformation (IDFT). One writes $y = (y_0, ..., y_{N-1}) \mapsto c = (c_0, ..., c_{N-1})$.

$$\text{DFT}: \; c_k = \frac{1}{N} \sum_{j=0}^{N-1} y_j e^{-i\frac{2\pi}{N}kj}, \quad k = 0, 1, ..., N-1 \tag{6.21}$$

$$\text{IDFT}: \; y_j = \sum_{k=0}^{N-1} c_k e^{i\frac{2\pi}{N}jk}, \quad j = 0, 1, ..., N-1 \tag{6.22}$$

In the special case that $N = 2^m, m \in \mathbb{N}$ holds, there is a algorithm called Fast Fourier Transform invented by Cooley and Tukey in 1965 [31]. It reduces the numerical effort of the DFT dramatically and instead of N^2 matrix multiplication one ends up with $\frac{N}{2}\log_2(N)$. Applying this theory on our initial wave function in momentum space $\psi(n)$ we can easily compute its Fourier transform in angle space and we obtain:

$$\psi(l) = \left(\mathcal{F}[\hat{\psi}(\theta)]\right)_l = \frac{1}{N} \sum_{j=1}^{N} \psi(\theta_j) e^{-i\frac{2\pi}{N}lj} \tag{6.23}$$

$$\hat{\psi}(\theta_j) = \left(\mathcal{F}[\psi(n)]\right)_l = \sum_{l=1}^{N} \psi(l) e^{i\frac{2\pi}{N}jl} \tag{6.24}$$

In fig. 6.1 we show an example of a Gaussian state in momentum representation and its Fourier transform in angle space as it was implemented in the numerical codes and routines.

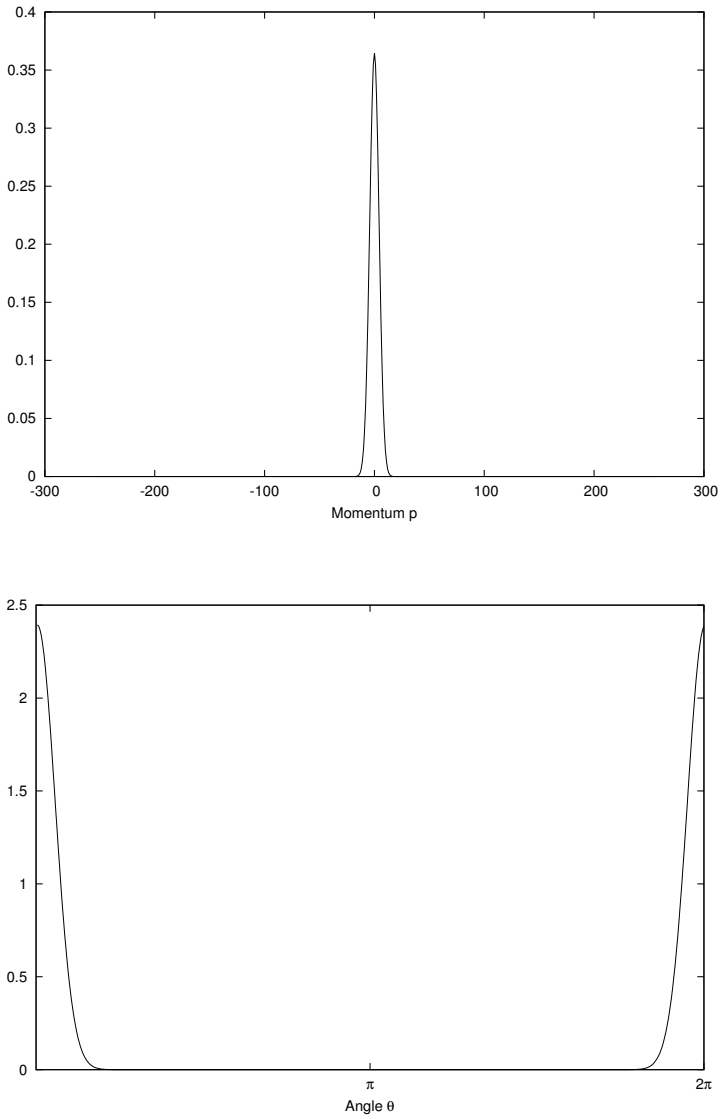

Figure 6.1: Plots of the initial wave function in momentum representation (upper figure) and its Fourier transform in angle space (lower figure). The angle-representation state is "centered" around the origin in the zone $[-\pi, \pi)$.

Bibliography

[1] S. Fishman; I. Guarneri; L. Rebuzzini. A theory of quantum accelerator modes in atom optics. *Physics*, 110:p. 16, 2002.

[2] A.J. Lichtenberg and M.A. Lieberman. *Regular and Chaotic Dynamics*. Number 38 in Applied Mathematical Science. Springer-Verlag, Berlin, 2nd edition, 1992.

[3] M. Hénon and C. Heiles. The applicability of the third integral of motion: Some numerical experiments. *Astron. J.*, 69:73–79, 1964.

[4] M. Gutzwiller. Quantum chaos. *Scientific American*, January 1992.

[5] B. V. Cirikov. A universal instability of many-dimensional oscillator systems. *Physical Reports*, 263, 1979.

[6] S. Fishman. Quantum localization in quantum chaos, 1993. Proc. of the International School of Physics "Enrico Fermi".

[7] S. Fishman; D. Grempel and R. Prange. *Phys. Rev. Lett.*, 49(509), 1982.

[8] F. L. Moore; J. C. Robinson; C. F. Bharucha; Bala Sundaram and M. G. Raizen. Atom optics realization of the quantum δ-kicked rotor. *Phys. Rev. Lett.*, 75:4598–4601, 1995.

[9] M. Sadgrove and S. Wimberger. Pseudo-classical theory for directed transport at quantum resonance. *New J. Phys.*, (083027), 2009.

[10] G. Casati; B.V. Chirikov; F.M. Izraelev; J.Ford. *Stochastic Behaviour of a Quantum Pendulum*. Number 93 in Lecture Notes in Physics. Springer-Verlag, Berlin, 1979.

[11] E. Ott. *Chaos in Dynamical Systems*. Cambridge University Press, Cambridge, UK, 2002.

[12] S. Wimberger. Lecture notes on nonlinear dynamics and quantum chaos. University of Heidelberg, Summer term 2012.

[13] H. Ammann; R. Gray; I. Shvarchuck; N. Christensen. Quantum delta-kicked rotor: Experimental observation of decoherence. *Physical Review Letters*, 80:4111–4115, 1998.

[14] H. Ammann; R. Gray; I. Shvarchuck; N. Christensen. Experimental observation of dynamical localization and decoherence in the atomic δ-kicked rotor. *J. Phys. B*, 31:2449–2455, 1998.

[15] C. F. Bharucha; J. C. Robinson; F. L. Moore; Quian Niu; Bala Sundaram and M. G. Raizen. Dynamical localization of ultracold sodium atoms. *Phys. Rev. E*, 60:3881–3895, 1999.

[16] M. Sadgrove; S. Wimberger. *A Pseudoclassical Method for the Atom-Optics Kicked Rotor: from Theory to Experiment and Back*, volume 60, pages 315–369. Academic Press, 2011.

[17] M. Abramowitz and I.A. Stegun. *Handbook of mathematical functions with formulas, graphs and mathematical tables.* Dover Publications, New York, 1964.

[18] J.J. Sakurai. *Modern Quantum Mechanics.* Addison-Wesley, New York, 1st edition, 1985.

[19] S. Wimberger; I. Guarneri; S. Fishman. Quantum resonances and decoherence for δ-kicked atoms. *Nonlinearity*, 16(1381), 2003.

[20] William H. Press; Saul A. Teukolsky; William T. Vetterling and Brian P. Flannery. *Numerical Recipes - The Art of Scientific Computing.* Cambridge University Press, Cambridge, UK, 3rd edition, 2007.

[21] K. Meyberg; P. Vachenauer. *Hoehere Mathematik 2.* Springer-Verlag, Berlin, 3rd edition, 1999.

[22] H. Kasten. Lecture notes on complex analysis 1. University of Heidelberg, Summer term 2012.

[23] M. J. Davies; Eric J. Heller. Quantum dynamical tunneling in bound states. *J. Chem. Phys.*, 246, 1981.

[24] P. Schlagheck; O. Brodier ; D. Ullmo. Resonance-assisted tunneling. *Annals of Physics*, 300(1):88–136, 2002.

[25] Immanuel Bloch, Jean Dalibard, and Wilhelm Zwerger. Many-body physics with ultracold gases. *Rev. Mod. Phys.*, 80:885–964, Jul 2008.

[26] S. Wimberger; M. Sadgrove; S. Parkins and R. Leonhardt. Experimental verification of a one-parameter scaling law for the quantum and "classical" resonances of the atom-optics kicked rotor. *Phys. Rev. A*, 71(053404), 2005.

[27] M. Sadgrove; S. Wimberger; S. Parkins; and R. Leonhardt. Ballistic and localized transport for the atom optics kicked rotor in the limit of vanishing kicking period. *Phys. Rev. Lett.*, 94(174103), 2005.

[28] S. Wimberger. *Chaos and Localisation: Quantum Transport in Periodically Driven Atomic Systems.* PhD thesis, Ludwig-Maximilian-University of Munich and Universit'a degli Studi dell' Insubria Como, 2004.

[29] F. Grossmann; T. Dittrich; P. Jung; P. Haenggi. Coherent destruction of tunneling. *Phys. Rev. Lett.*, 67(4):516–519, 1991.

[30] A. Tomadin. Quantum chaos with ultracold atoms in optical lattices, 2006. Diploma thesis.

[31] James W. Cooley and John W. Tukey. An algorithm for the machine calculation of complex fourier series. *Math. Comput.*, 19:297–301, 1965.

Acknowledgements

Finally, in the end of this bachelor thesis, I want to thank some people who supported me during the past five months.

First of all, I want to thank my supervisor Sandro Wimberger who introduced the topic of the quantum kicked rotor in position space to me. He was always open for my questions and had lots of advice for me. I learned very much from him during my work on this topic and I am grateful for having shared his enthusiasm.

I thank Prof. Komnik for correcting this thesis together with Sandro Wimberger and for examining me in the final colloquium.

Another thank goes to Prof. Ulf Peschel and Christoph Bersch from the Friedrich-Alexander-University of Erlangen who provided us with lots of exciting experimental data on light signals in optical fibers.

In Heidelberg I, want to say thank you to Carlos Parra-Murillo, Matthias Kraft and Stephan Burkhardt who helped me finding lots of mistakes in this thesis and provided me with so much technical advise in physics and programming. I also thank Georgios Kordas for the opportunity of integrating my knowledge about the kicked rotor into the solutions of the tutorials in the quantum chaos course.
Finally, thanks to all members of the group Julia, Sandro, Anton, Georgios, Carlos, Matthias and Stephan I had an amazing semester at the Institute for Theoretical Physics and very sporty wednesdays full of football at the Neckarwiese.

Last but not least a big thank goes to my parents. They supported me during my bachelor's and were behind me during all its highs and lows. For this and their love, I am very grateful.

Erklärung

Ich versichere, dass ich diese Arbeit selbstständig verfasst und keine anderen als die angegebenen Quellen und Hilfsmittel benutzt habe.
Heidelberg, den ...,